Biosensors and Bioelectronics 170 (2020) 112663

Contents lists available at ScienceDirect

Biosensors and Bioelectronics

journal homepage: http://www.elsevier.com/locate/bios

Label-free brain tissue imaging using large-area terahertz metamaterials

Sang-Hun Lee [a], Seulgi Shin [b,c], Yeeun Roh [a,d], Seung Jae Oh [e], Soo Hyun Lee [a], Hyun Seok Song [a], Yong-Sang Ryu [a], Yun Kyung Kim [b,c], Minah Seo [a,f,*]

[a] Sensor System Research Center, Korea Institute of Science and Technology, Seoul, 02792, Republic of Korea
[b] Convergence Research Center for Diagnosis, Treatment and Care System of Dementia, Korea Institute of Science and Technology, Seoul, 02792, Republic of Korea
[c] Division of Bio-Medical Science & Technology, KIST School, Korea University of Science and Technology (UST), Seoul, 02792, Republic of Korea
[d] Display and Nanosystem Laboratory, College of Engineering, Korea University, Seoul, 02841, Republic of Korea
[e] YUHS-KRIBB Medical Convergence Research Institute, College of Medicine, Yonsei University, Seoul, 03722, Republic of Korea
[f] Division of Nano & Information Technology, KIST School, Korea University of Science and Technology (UST), Seoul, 02792, Republic of Korea

ARTICLE INFO

Keywords:
Metamaterial
Terahertz
Imaging
Amyloid beta
Biosensor

ABSTRACT

Terahertz (THz) imaging technology has shown significant potential for use in biomedical imaging owing to its non-ionizing characteristics by its low photon energy and its ultrabroadband spectral comparability with many molecular vibrational resonances. However, despite the significant advantage of being able to identify biomaterials in label-free configurations, most meaningful signals are buried by huge water absorption, thus it is very difficult to distinguish them using the small differences in optical constants at THz regime, limiting the practical application of this technology. Here, we demonstrate advanced THz imaging with enhanced color contrast by the use of THz field that is localized and enhanced by a nanometer-scale slot array. THz images of a biological specimen, such as mouse brain tissue and fingerprint, on a nano-slot array-based metamaterial sensing chip, which is elaborately fabricated in large-area, show a higher contrast and clearer boundary information in reflectance without any labeling. A reliable numerical solution to find accurate optical constants using THz nano-slot resonance for the quantitative analysis of target bio-specimens is also introduced. Finally, the precise optical properties of real bio-samples and atlas information are provided for specific areas where amyloid beta proteins, known to cause dementia, have accumulated in a mouse brain.

1. Introduction

Photonics has become an essential part of sensing and imaging research due to the advantage of improved optical materials based on cutting-edge nanotechnology. The unique optical behavior of nanoscale materials, for example, can help to overcome the limitation in device performance demonstrated by intrinsic bulk materials on a macroscopic scale. The performance of various optical techniques in the visible to the infrared range can be enhanced by combining them with subwavelength photonic structures on a nanoscale (Neubrech et al., 2017; Zeng et al., 2014). THz technologies have also benefited from the proliferation of semiconductor and metal fabrication techniques at a subwavelength scale below hundreds of microns (Kang et al., 2018). In particular, elaborately fabricated resonant structures such as metamaterials have shown great potential for use in molecule-specific sensing applications due to the enhanced sensitivity arising from the unique THz optical properties of specially designed nanostructures (Lee et al., 2019). Narrow metallic gap structures with a nanoscale width exhibit remarkable electric field enhancement inside a hot spot area while the magnetic field remains almost intact (Seo et al., 2009). This asymmetric field amplification leads to light-matter interaction with a greater quantum mechanical absorption cross-section mitigating the bottleneck in sensitivity for the sensing of chemicals at very low concentration (Park et al., 2013).

Many molecules have exotic resonances that can be used as spectral fingerprints because the THz photon energy corresponds to the intra- and inter-molecular dynamics. By matching the molecular resonances and metamaterial resonances within this frequency regime, a particular molecule can be distinguished from other substances that have a very similar molecular structure (Alfihed et al., 2020; Geng et al., 2017; Lee et al., 2015, 2019; Qin et al., 2016; Serita et al., 2018; Xu et al., 2019; Yan et al., 2019). In previous studies, biological analytes such as steroids (Lee et al., 2019), viruses (Lee et al., 2017), DNA (Lim et al., 2018), and other biochemicals (Lee et al., 2015; D.-K. Lee et al., 2018; Wu et al.,

* Corresponding author. Sensor System Research Center, Korea Institute of Science and Technology, Seoul, 02792, Republic of Korea.
E-mail address: mseo@kist.re.kr (M. Seo).

https://doi.org/10.1016/j.bios.2020.112663
Received 19 August 2020; Received in revised form 21 September 2020; Accepted 28 September 2020
Available online 28 September 2020

2013) have been sensitively and selectively discriminated using slot-antenna resonance structures by matching their THz absorption fingerprints. For example, the optical properties of diluted avian influenza viruses have been intensively examined and the subtypes identified, thus offering a rapid diagnostic method for time-sensitive bio-materials, such as high-throughput screening (HTS) (Lee et al., 2017). For real biological applications, however, unavoidable absorption by the aqueous environment inside the target tissue within the THz regime has been a significant issue. In THz imaging technology, signal errors, and deformation due to water absorption, which has an absorption coefficient of 240 cm^{-1} at 1 THz, should be carefully considered (Meng et al., 2014; Rahman et al., 2016). Therefore, for *in situ* imaging, a novel strategy is required to effectively differentiate the low optical signal of the real target from the underwater absorption.

Here, we present an advanced THz imaging platform that employs nano-slot structured metamaterials to produce a higher image contrast and increased sensitivity. A nano-slot array was uniformly fabricated on a centimeter-scale for the large-area imaging of real bio-samples. THz images of brain tissue on the nano-slot array exhibited a noticeably higher image contrast compared to images on an unpatterned Si substrate, which represents the conventional THz imaging approach. For the quantitative analysis of the THz images and the extraction of accurate optical constants, a reliable calculation model was developed by comparing changes in the signal for various analytes with the fundamental spectrum for the nano-slot array. The complex refractive indices extracted for the tested mouse brain tissue allowed the development and progression of dementia in the mouse brain to be monitored. Enhanced THz imaging using nanoscale metamaterials and an accurate extraction algorithm for the complex refractive indices can be useful for use in broadly defined optical biosensors, including the monitoring of disease in a label-free manner.

2. Experimental section

2.1. THz measurement

The THz system based on conventional time-domain spectroscopy is driven with a Ti:sapphire femtosecond laser, which has 800 nm of center wavelength, 100 fs of pulse width, and 80 MHz of repetition rate. The laser is divided into two parts for THz emission and detection with an optical delay line. THz waves generated by the photoconductive antenna are guided by imaging module, which consists of metallic mirrors, a Si beam splitter, and TPX (Polymethylpentene) lenses, for perpendicular incidence to the sample. Reflected THz waves are measured by the electro-optic sampling method using ZnTe crystal. The reference signal was measured using a metallic mirror on the sample stage (Supplementary Fig. 1). The signal-to-noise ratio reaches to 60 dB, even including signal loss by Fresnel losses from the substrate and the imaging module. For two-dimensional imaging using the single-pixel detector, the samples were mounted on a motorized *x-y* stage and raster-scanned pixel-by-pixel, with careful alignment to avoid undesirable tilt that may produce a temporal delay in the THz pulse and signal loss due to defocusing (Supplementary Fig. 2). The reflectance is defined as $R(\omega) = |E(\omega)/E_{ref}(\omega)|^2$, where E and E_{ref} are the reflected signals from the sample and a metallic mirror as a reference, respectively.

2.2. Design and fabrication of THz nano-slot chip

To accurately quantify the optical constants of the target sample, the ability to mass-produce metamaterial-based sensing chips with numerous identical nano-slots is essential. For this purpose, a large-area nano-slot array was fabricated as a sensing chip using photolithography on a 6-inch wafer. The patterned wafer was cut into 2 cm × 2 cm sections, to match the size of the sectioned mouse brain. The nano-slot array is fabricated using photolithography technique on high resistivity Si wafer to avoid absorption-loss (>10,000 Ωcm, 675 μm thickness). The thickness of Au film is 150 nm, which is thicker than the skin depth, for suppressing direct transmission and measurement of clear resonance (Jeong et al., 2019). The elementary nano-slot was designed to have a resonance frequency, f_{res} (length $l = 60$ μm), that was close to the highest signal-to-noise ratio of the incident THz spectrum, as following the relation: $f_{res} = c_0/\sqrt{2l(n^2+n_s^2)}$, where c_0 is the speed of light, and n and n_s are the refractive indices of the medium and the Si substrate, respectively (Kang et al., 2009). The selected width also represented a compromise in that it reflected the minimum size for which the quality of the edge and the high aspect ratio of the nano-slot array could still be guaranteed for the photolithography technique used in the fabrication process (Supplementary Fig. 3). The individual nano-slots were periodically arranged with transversal ($P_x = 40$ μm), and longitudinal ($P_y = 10$ μm) separations between neighboring nano-slots to eliminate the Rayleigh minima (Lee et al., 2007).

2.3. Preparation of the brain tissue sample

The mouse brain for THz imaging with the nano-slot was prepared as shown in Supplementary Fig. 4. The brain of C57BL/6 and APP/PS1 mice were perfused with 0.9% saline, then was extracted and fixed by 4% paraformaldehyde solution. After cryoprotection in the 30% sucrose solution, the brains were frozen in optimal cutting temperature (OCT) compound. The coronal section of the mouse brain at -1.94 mm posterior to the bregma, which was cut using freezing microtome with 30 μm thickness, was placed on the top of both substrates of the bare Si substrate and the nano-slot chip. To prevent deformation by dehydration, the tissue was covered by mounting solution (Dako, s3023) and a cover glass with sealing along the edge. The sectioned brain tissue was then placed on a nano-slot chip, covered by mounting solution, and sealed to prevent deformation due to dehydration.

2.4. H&E stain and Thioflavin S stain

For H&E stain, brain tissue slices mounted on a glass slide were immersed in Hematoxylin solution (Gill No. 1) for 5 min. Then, the slide was soaked into 40% acetic acid and counterstained with Eosin Y solution (5 wt % in H_2O) for 2 min. The slices were dehydrated with graded ethanols (70, 80, 90, and 100%) and xylene (100%). Then, the brain tissue slices were mounted with DPX mounting medium (Sigma) and imaged by using a Ti microscope (Nikon).

For the visualization of amyloid beta (Aβ) plaques, the brain tissues of APP/PS1 mice were stained with 10 μM of Thioflavin S (ThS) for 30 min. After washing with phosphate-buffered saline (PBS) for 10 min, brain tissue slices were mounted with fluorescence mounting medium (Dako) and imaged by using Axio Scan. Z1 (Zeiss).

3. Results and discussion

3.1. Nanoscale metamaterial fabrication and THz experiments

For sensitive imaging of brain tissue with a nano-slot array, we exploited a THz time-domain spectroscopy (TDS) system in reflection mode, as described in Fig. 1A. Reflection measurements were used to reduce the signal loss caused by water absorption. The prepared brain tissue of a C57BL/6N mouse was frozen in an optimal cutting temperature (OCT) compound and sectioned at a thickness of 30 μm, corresponding to λ/10 (a center wavelength at 1 THz is 300 μm). It is important to note that the organ structure or boundaries of thin brain tissue samples cannot be clearly seen without staining (transparent inset images in Fig. 1a).

Recent research has introduced strategies that allow the THz optical properties of a small quantity of analyte to be extracted and quantitatively characterized using nano-slot-based metamaterials (Lee et al., 2020; Lim et al., 2018). One efficient method is based on fitting the

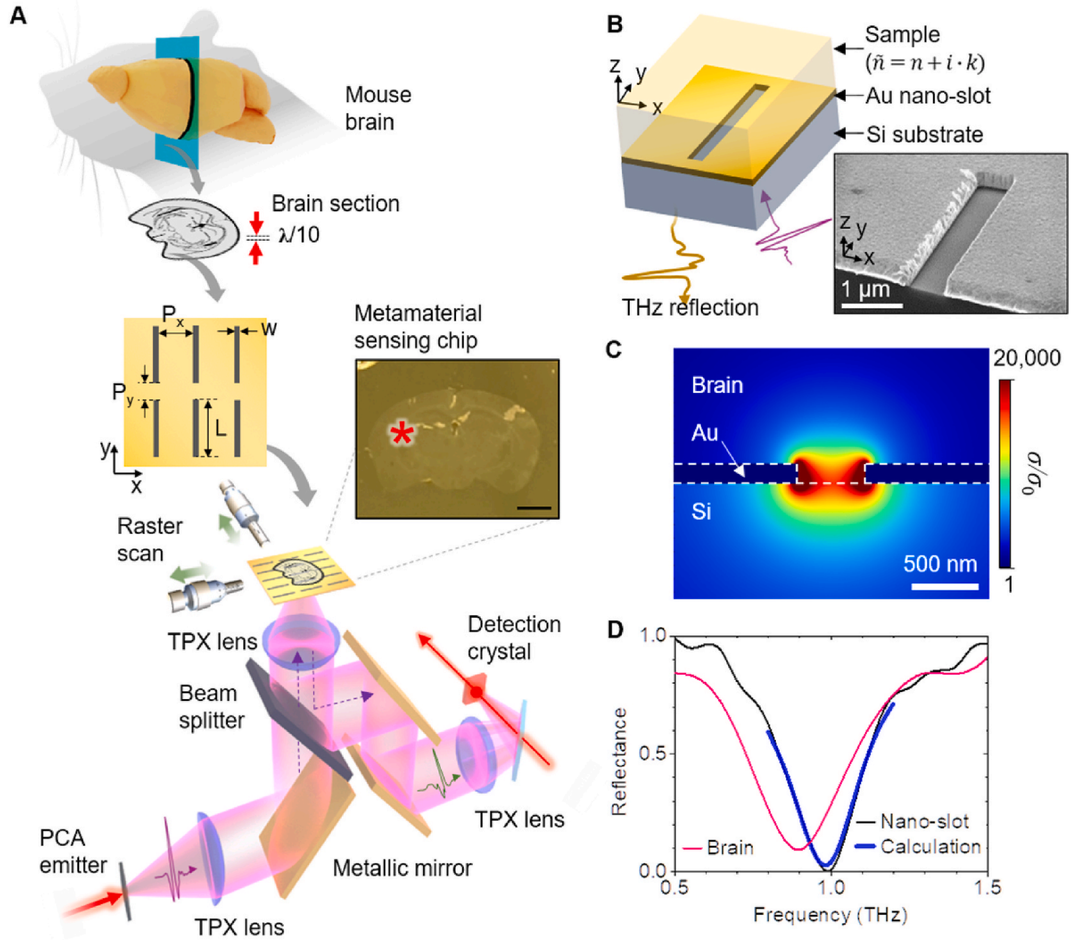

Fig. 1. Advanced THz imaging system. (A) THz spectroscopy setup for reflection imaging with sectioned mouse brain tissue placed on a nano-slot-array-based sensing chip. Inset is an image of the brain tissue attached to the metamaterial sensing chip. The scale bar represents 2 mm. (B) Schematic diagram of the nano-slot surrounded by the dielectric medium used for calculation. Inset is an SEM image of an enlarged individual nano-slot at the cut-edge. (C) Calculated cross-sectional distribution of the field enhancement near a nano-slot, which is based on the diagram described in B. (D) THz reflection spectra for the nano-slot array with and without brain tissue. The THz spectrum for the brain sample was obtained at the position marked in the inset in A.

calculated transmission spectra to experimental results to determine the permittivity and conductivity of the tested analyte. This has the benefit of access to the full range of spectral information to accurately determine the optical constants for the sample, but data processing for 2-dimensional (2D) images with numerous pixels is burdensome. For this reason, a simplified and specific computation technique is employed in the present study to efficiently process the 2D image data. Using the finite element method (FEM) simulations based on the geometry of Fig. 1B, which represents an elementary slot, the reflection spectra for the slot surrounded by arbitrary media with certain refractive indices were calculated. The Drude parameters of the metal film were determined by the spectral fitting of the measured reflectance for the bare nano-slot array with the already-known optical properties of air ($n = 1$) and Si ($n = 3.41$). The width (w) of each nano-slot (500 nm) leads to an electric field enhancement factor of 300 (Roh et al., 2019). The significantly enhanced THz field near the nano-slot was also captured by the simulations (see Supplementary Fig. 5). The field enhancement can be directly converted to an increase in the molecular cross-section (σ) via a large absorption coefficient, proportional to the ratio of the electric and magnetic fields ($\sigma \propto E^2/S$, where E and S are the electric field and the Poynting vector, respectively) (Park et al., 2013). The enhanced ratio of molecular absorption cross-section (20,000 for a specific medium such as brain tissue) allows for highly sensitive probing (Fig. 1C). The resonant reflectance measured for the bare nano-slot array is plotted in black in Fig. 1D, with the spectrum suggested by the model plotted in blue, demonstrating good agreement. In the experimental analysis, the resonance spectrum of the nano-slot array was altered by the brain tissue sample (plotted in magenta), thus reflecting the optical properties of the sample.

3.2. *Characterization of optical properties for various media with nano-slots*

When measuring trace biochemical samples using nano-slots, it has been already verified that THz near-field enhancement by the nano-slots leads to very strong molecular absorption by the samples as described in Fig. 1C and several earlier studies (Lee et al., 2015, 2019; Park et al., 2013). To determine the effect of THz field enhancement by nano-slots on the image contrast, several real bio-samples were first imaged using nano-slots in the reflectance configuration. A wet sagittal section from a mouse cerebellum was prepared without fixation (cross-sectional view of photograph image in Fig. 2A). The cerebellar cortex had a darker color compared to the inner region of the cerebellum, representing gray matter consisting of cell bodies and capillaries. The arborvitae appeared white because of the myelin sheath surrounded by nerve fibers. The THz reflectivity of white matter is known to be only 2% higher than that of gray matter in paraffin-embedded tissue samples (Yeo et al., 2017). In contrast, in wet samples under purely natural conditions, distinguishing between white and gray matter is considered almost impossible due to interference from the water absorption signals. However, the THz image

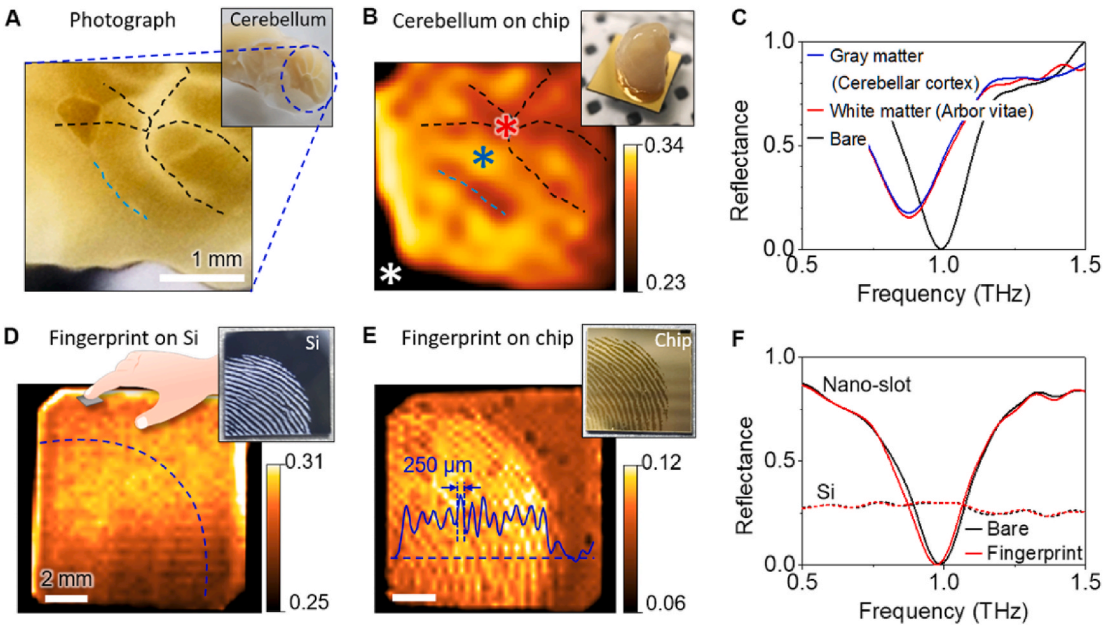

Fig. 2. High contrast THz images using nano-slot array. (A) Photographic image of a sagittal cross-section of mouse brain tissue and (B) a THz image using a nano-slot array. The inset in A and B show an image of the sagittal cross-section of the whole brain on a transparent glass and on a nano-slot chip, respectively. The black dashed lines indicate the white matter that appears in both figures. Blue dashed line indicate ventricle. (C) Reflectance spectra for gray matter (blue), white matter (red) regions, and a nano-slot chip (black) from points with their corresponding color in B. THz image of a real fingerprint with (D) a bare Si substrate and (E) a nano-slot chip. Inset in D and E is an image of the fingerprint on each chip. The dashed blue line in D indicates the edge of the fingerprint. The cross-sectional reflectance extracted from the dashed blue line in E shows the FWHM of the fingerprint pitch. (F) Reflectance spectra for real fingerprints (red) with bare Si (black) and a nano-slot array. (For interpretation of the references to color in this figure legend, the reader is referred to the Web version of this article.)

using nano-slots, obtained at 0.95 THz near the resonance, clearly distinguishes between the two areas (Fig. 2B), with a 4% difference in the reflectance spectrum between the two (Fig. 2C). Due to the flexibility of the brain tissue, the shape of the ventricle marked in blue dashed line can be changed in the process of attaching onto the nano-slot array. This reflects enhanced THz signals around the nano-slots, which allows the very small variation in the refractive index on the surface of the brain sample to be detected. The higher intensity of the contrast in the THz image was also observed in extremely thin bio-samples. THz reflection images were obtained from real human fingerprints with and without the use of a nano-slot array. Using a conventional THz source at 1 THz (300 μm wavelength), information on the fingerprint patterns could not be obtained (Fig. 2D). It is noted that the imprinted fingerprint patterns are on average 263 nm thick, which is below λ/1000 at 1 THz (see Supplementary Fig. 6). Interestingly, the fingerprint pattern was clearly captured using nano-slots with a resonance at 1 THz, with the pitch of the fingerprints on average about 250 μm apart, corresponding to the diffraction limit of the THz wave (Fig. 2E). The enhanced contrast of the

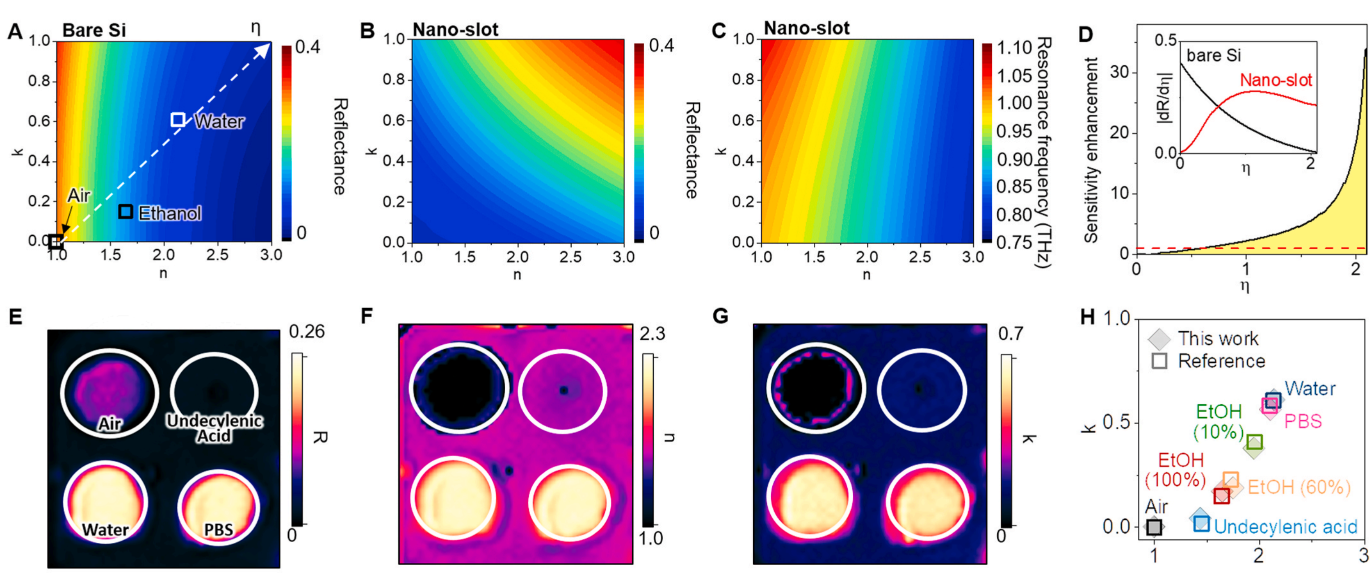

Fig. 3. Quantification of the THz optical characteristics of various media with the nano-slot array. Changes in the reflectance due to the dielectric medium attached to (A) bare Si and (B) a nano-slot. (C) Changes in the resonance frequency of the nano-slot array. (D) Sensitivity enhancement of the nano-slot array. The inset presents the sensitivities of the sensing chip and substrate. (E) THz reflection images of four phantoms. Extracted (F) *n* and (G) *k* images of the phantoms, respectively. (H) Summarized refractive indices of various analytes.

image was the result of a shift of 0.011 THz in the resonance ($\Delta f/f_{res}$ = 1.1%) in the reflectance spectrum (the solid lines in Fig. 2F), while there was no meaningful difference in the signal due to the fingerprint on the bare Si substrate (the dashed lines in Fig. 2F). The negligible change in the amplitude of the reflection means that the tested fingerprint had extremely low traces of skin, which is rarely detected by THz waves. Variation in the change in the spectral shape between samples means that there were complex and sophisticated mechanisms underlying the enhancement of the image contrast. Based on these results, the absolute optical constants were extracted and analyzed to quantify the image enhancements (Kang et al., 2009).

The change in amplitude of reflectance (ΔR) and the resonance frequency shift (Δf) were measured in the THz signal to extract the refractive indices of the attached dielectric media. When a dielectric medium is attached to a bare Si substrate without a nano-slot pattern, the THz reflectance can be simply determined by the Fresnel equation (Fig. 3A). The range of the complex refractive index ($n + ik$) covers most ordinary dielectric materials including air, water, and ethanol, as indicated in the dispersion graph. However, when imaging using nano-slots, it is challenging to accurately calculate the THz reflectance due to its complicated resonance behavior arising from the antenna-like structure of the nano-slot. Thus, we used an FEM simulation model and analyzed the spectrum in terms of the resonant reflectance based on the scheme introduced in Fig. 1B. The distribution of the reflectance for the nano-slot array is plotted in Fig. 3B. In addition, the changes in the resonance frequency of the nano-slot array in terms of complex refractive indices are summarized in Fig. 3C, which shows strong dielectric material-dependence. Using the distribution results, the changes in reflectance by the analytes on the sensing substrate can be analyzed both qualitatively and quantitatively. The sensitivity of both sensing substrates can be considered in terms of the change in reflectance using η ($\eta = \sqrt{(n-1)^2 + k^2}$), which corresponds to the change in the refractive index along the dashed line in Fig. 3A. The enhancement in sensitivity by the nano-slot array compared to the bare Si can be defined according to the following equation: Sensitivity enhancement $= \frac{|dR_{nano-slot}/d\eta|}{|dR_{Si}/d\eta|}$. The enhancement in sensitivity of the nano-slot array exponentially increased as the refractive index increased (Fig. 3D). The inset figure displays the sensitivity ($|dR/d\eta|$) of the nano-slot array and the bare Si substrate in terms of η. The nano-slot array exhibited higher sensitivity than the bare Si at $\eta \geq 0.58$ ($n = 1.58$, $k = 0.262$), which covers most dielectric media and wet biological tissue samples.

To verify our suggested model, we measured the THz reflection images for several phantom target materials placed on a nano-slot sensing chip (Fig. 3E). Double-sided adhesive tape with four punched holes was attached to the chip, and phantom materials were placed in each hole, and then sealed with polydimethylsiloxane (PDMS) film. One sample was air as a control. Undecylenic acid, which was used to imitate fat tissue, is a colorless oil of an unsaturated fatty acid and widely used in the manufacture of pharmaceuticals. Deionized water and phosphate-buffered saline (PBS) were tested as alternative forms of human or animal soft tissue of human or animal. Because both the reflectance (R) and the resonance frequency (f_{res}) of the nano-slot array influence the determination of n and k for the attached medium, it is important to find a specific value that satisfies the optimal conditions at the same time in the two maps, $R(n, k)$ and $f_{res}(n, k)$. By finding a coordinate (the complex component of the refractive index in Fig. 3B and C) that minimizes the difference between the measured and calculated values in the maps for R and f_{res}, the refractive index of each pixel that includes the individual THz spectrum is extracted (see Supplementary Fig. 7). In the respective region in Fig. 3F and G, the color is almost uniformly distributed in both images for n and k, which means that the model developed to determine the complex refractive index using nano-slot resonance exhibited high reliability. The refractive indices for the four targets extracted by the model (minimization of the difference in resonance) are summarized in Fig. 3H with additional measurements for aqueous ethanol (EtOH) solutions with various molar concentrations. All of the complex refractive indices extracted from the models show good agreement with conventional THz-TDS measurements (see Supplementary Fig. 9) and the previously published data (Bowman et al., 2019; Kitahara et al., 2005; Oh et al., 2013).

The resonant reflectance (R) and frequency (f_{res}) information in the extraction of optical constants can produce accurate refractive indices for both complex parts, reducing the processing time. For example, to produce the maps for R and f_{res} in Fig. 3B and C using the proposed minimization of the difference in resonance, the spectra were calculated in 231 cycles (21 × 11 FEM calculations, 0.1 steps in the n and k range, respectively). Additional time costs, such as those required to find the optimized refractive index, are negligible compared to the simulations. Full spectral fitting for all of the pixels in an image requires many calculation cycles. In our approach, as an example, spectral fitting near the resonance frequency requires the calculation of 63 cycles for a single pixel. Consequently, the suggested method is beneficial in reducing the computational costs when processing a large volume of data, which is required for THz images. In addition, this method can be generally applied to other metamaterials with different structures.

3.3. THz imaging of mouse brain tissue

Using the proposed model and imaging platform, mouse brain tissue was imaged and analyzed. Three continuously sectioned mouse brain slices were prepared with almost identical cross-sectional views. Because a brain section is almost transparent under visible light, staining with hematoxylin and eosin (H&E) is generally employed to distinguish structures. The optical microscope image in Fig. 4A shows the brain anatomy according to differences in cell density. Two sections were transferred onto the bare Si substrate and nano-slot array and imaged, respectively. THz reflectance images taken at 0.95 THz, which is near the resonance frequency of the nano-slot array, are presented. The image acquired using the bare Si substrate did not clearly show boundaries between different structures (Fig. 4B) due to the thin sample (30 μm) and the multiple reflections, as was also observed with the fingerprint results (Fig. 2D). Given that the sample was approximately 1 cm in size and the spatial resolution was determined by the diffraction limit of a THz wave, the quality of the image appeared equal to that of the conventional THz system. This challenging bio-sample in terms of size, thickness, and material components was then examined with a nano-slot sensing chip. The colors for the image when taken using the nano-slot array were inverted when compared to the Si substrate because the amplitude of the reflection increased as the refractive index increased, and it was much higher on the gold metal side. Due to the strong contrast, a stronger color difference and clear boundaries in the image were obtained using the nano-slot chip (Fig. 4C), with the resonances shifted to different degrees for specific regions (Fig. 4D). The THz image clearly distinguishes certain regions of the brain: white matter (corpus callosum) has a lower reflection amplitude than gray matter, including the thalamus and hypothalamus. Compared to the bare Si image, which only faintly depicted the brain anatomy, such as the cerebral cortex and thalamus, the contrast in the nano-slot image was noticeably higher. The cross-sectional values along the dashed lines a and b in Fig. 4B and C are summarized in Fig. 4E and F. The yellow, blue, and green areas in Fig. 4E correspond to the cerebral cortex, corpus callosum, and hypothalamus, respectively. In the same area of the brain tissue, the nano-slot had a 2.4 (line a) and 4 (line b) times higher change in reflectance, leading to the strong imaging contrast.

The reflectance of tissue in the THz region can be modified by the constituents (Darmo et al., 2004; K. Lee et al., 2018). In particular, gray matter, including the cortical cortex and thalamus, has a high protein content with a large amount of water, producing a higher refractive index and greater absorption. In contrast, white matter, such as the corpus callosum, is mainly composed of myelinated axons. Because fatty substances have a lower refractive index and absorption than water,

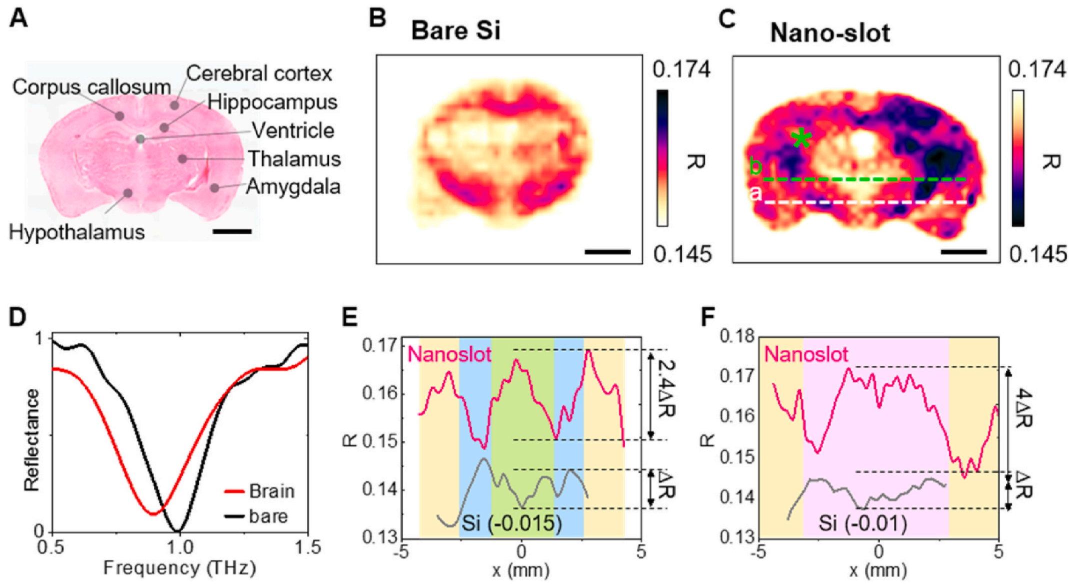

Fig. 4. The THz imaging results of mouse brain tissue. (A) H&E stained image of a mouse brain tissue. THz reflection images using (B) a bare Si substrate and (C) a nano-slot chip. (D) Reflectance spectra for the points marked in C and a bare nano-slot chip. Reflectance values along the dashed lines (E) a and (F) b from images B and C.

white matter tends to produce less of a change in reflectance and resonance shift (Darmo et al., 2004; Kang et al., 2009). This effect on the image contrast of water, lipids, and other proteins can be compared to magnetic resonance imaging (MRI) (Shmueli et al., 2011). Due to differences in the magnetic relaxation behavior of protons in the amide and hydroxyl groups of water, lipids, and proteins, specific areas of the brain can be distinguished. Because of the strong relation between the image contrast and the constituents of a specimen, the THz image in Fig. 4C displayed a very similar internal structure to that seen in MRI (see the images −2 mm from bregma in Ref (Lee et al., 2012).).

3.4. THz monitoring of an Alzheimer's disease model

Analysis of the THz optical responses from tissue using metamaterials can be utilized as a diagnostic method for brain diseases, such as cancer or dementia, that lead to structural and/or chemical changes. An Alzheimer's disease mouse model (APP/PS-1) was investigated using the proposed THz metamaterial-based system and compared with those Thioflavin S fluorescence staining for Aβ peptide, which is crucially involved in Alzheimer's disease due to toxicity to nerve cells. Brain sections from 4-month to 10-month old mice were prepared and THz reflection images were taken in the same way as shown in Fig. 4. To observe surface changes in Aβ aggregation, brain slices of wild type and the APP/PS1 mice were placed on left- and the right-side, respectively. Extracted THz refractive index images at each age are plotted in Fig. 5A. Because the major component of a fresh brain over 80%, is water, and other components contribute together to the detailed image contrast (Agrawal et al., 1968), the brain tissue on the nano-slot also has a very similar refractive index with water (See Supplementary Fig. 7) (K. Lee et al., 2018; Yamaguchi et al., 2016). Due to its structure and constituent difference, images of the refractive index basically reflect shapes from the image of reflection in Fig. 4C. It is noted that the refractive indices of the APP/PS1 mice, especially in the cerebral cortex and hippocampus, are gradually decreased by age, while wild type mice show almost intact values. It is already known that Aβ plaque is mainly accumulated in the cerebral cortex and hippocampus because of the plentiful neuron population in these regions (Radde et al., 2006). To confirm our measurement, accumulation of Aβ plaque in the brain was monitored using the brain section at each stage with Thioflavin S staining and observation using a conventional fluorescence microscope (Fig. 5B). The number of green spots, which corresponds to Aβ aggregation, is gradually increased mainly in the cerebral cortex and hippocampus on 4- to 10-month-old mice, whereas there is no fluorescence spot on the brains of wild type mice (see Supplementary Fig. 10). Therefore, THz brain image reflects the development of Alzheimer's disease. To trace refractive index change on characteristic brain regions, we statistically summarized the refractive indices with extracted data on the region denoted in Fig. 5C. Red, green, and blue areas correspond to the cerebral cortex, hippocampus, and thalamus, respectively. On the cerebral campus in Fig. 5D, the refractive index of each age of wild type brain shows almost similar by age. Meanwhile, the APP/PS1 model of Alzheimer's disease shows noticeably decreasing the refractive index by aging. Hippocampus, in Fig. 5E, also shows similar relation with cerebral cortex; remarkable change in APP/PS1 and little difference in wild type of 4-, 7-, 10-month--old mice. Thalamus (Fig. 5F), which is a non-prominent area of Aβ plaque, depicts much smaller changes in the APP/PS1 mice that are comparable to wild type, unlike the cerebral cortex and hippocampus. Errorbars indicate the ranges of refractive index. Recently, it was reported that polymerizing of Aβ reduced its conductance, which corresponds to getting a lower refractive index (Heo et al., 2020). Particularly, fibrillized Aβ shows almost depressed conductance. This trend agrees well with our result that development of the Alzheimer's disease makes decreasing the refractive index of the brain tissue in the THz range. Therefore, it is emphasized that our advanced THz system, which can directly observe Aβ plague is fully expressed without dye staining, can be useful for diagnostic purposes with fully meaningful information.

4. Conclusions

In conclusion, we demonstrate a sensitive THz imaging technique for mouse brain tissue with nano-slot patterned metamaterials. Contrast-enhanced THz images with clearer boundaries were obtained as compared with previous reports (Darmo et al., 2004; Ji et al., 2016; K. Lee et al., 2018; Yun et al., 2017). Due to enormous THz field enhancement inside the nano-slot, sensitive THz image was acquired with an amplified reflection signal. The images represent a higher color contrast of 2.4–4 times compared to those with a conventional THz system. Because reflection spectra are not ruled by the simple Fresnel equation, for the direct extraction of complex optical constants for the

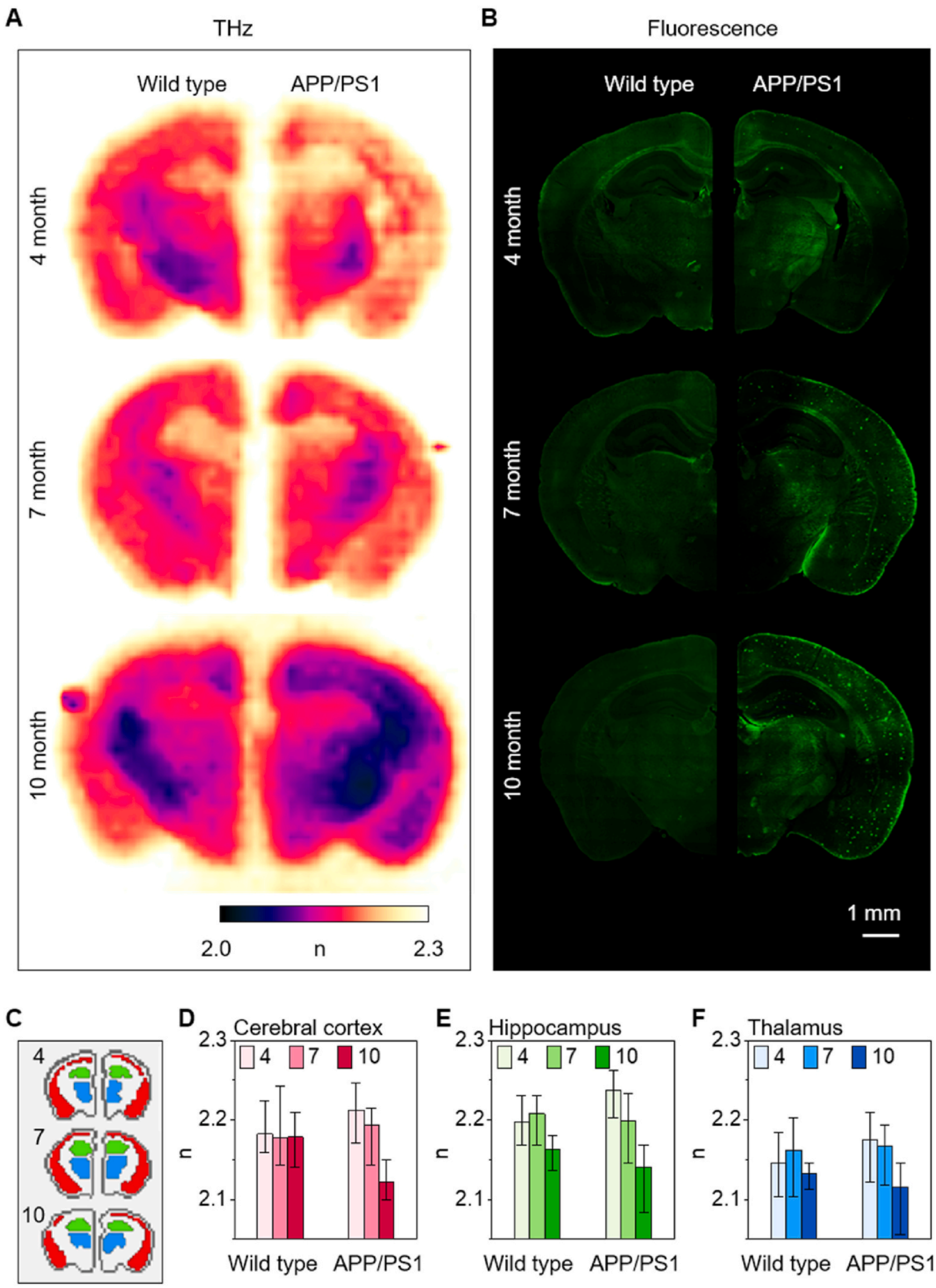

Fig. 5. THz refractive index images of a mouse model of Alzheimer's disease. (A) Refractive index images and (B) corresponding Thioflavin S stained images for 4-month to 10-month old mice. The images on the left are for wild type, while those on the right are APP/PS1 model for Alzheimer's disease. The averaged THz refractive indices at specific areas marked in (C) are summarized in (D) (red, cerebral cortex), (E) (green, hippocampus), and (F) (blue, thalamus). (For interpretation of the references to color in this figure legend, the reader is referred to the Web version of this article.)

nano-slot reflection spectra, therefore, modified FEM calculation method was introduced. The dispersion maps of real and imaginary parts of the refractive indices are composed for quantitative optical analysis of the specimen. They show an excellent agreement with the spectroscopic results in previous references. Based on the optimization algorithm, the THz images of mouse brain tissue in a real environment without dehydration process such as paraffin embedding were intensively analyzed. The THz obtained images of mouse brain tissue show their anatomy very similar to the known MRI results because contrasts in both imaging techniques are from the distribution of water, proteins, and fatty constituents. In this study, we demonstrate imaging techniques with a specimen in vitro as a proof-of-concept at the current stage. The sensitive imaging technique with THz near-field enhancement can be applied not only for soft tissues but also for rigid tissues such as bones by the development of a method overcoming the contact issue at the sensing surface. We hope that our result helps develop imaging technology that is available in the clinical field by combining with cutting-edge nanotechnologies related to the THz devices. These findings also may eventually lead to the development of non-invasive diagnostic imaging tools that are currently in high demand.

Author contributions

S.-H.L. and M.S. developed the concept of the work and wrote the paper. S.-H.L carried out THz experiments and FEM simulation with Y. R., S.J.O., and S.H.L. S.S. prepared samples with Y.K.K. H.S. S. and Y.-S. R. contributed to analyze experimental data and prepared figures. The manuscript was written through contributions of all authors. All authors have given approval to the final version of the manuscript.

CRediT authorship contribution statement

Sang-Hun Lee: Methodology, Software, Visualization, Investigation, Writing - original draft. **Seulgi Shin:** Resources, Formal analysis, Visualization. **Yeeun Roh:** Investigation. **Seung Jae Oh:** Resources, Validation. **Soo Hyun Lee:** Investigation. **Hyun Seok Song:** Resources. **Yong-Sang Ryu:** Visualization. **Yun Kyung Kim:** Validation, Resources, Conceptualization. **Minah Seo:** Conceptualization, Funding acquisition, Project administration, Supervision, Writing - review & editing.

Declaration of competing interest

The authors declare that they have no known competing financial interests or personal relationships that could have appeared to influence the work reported in this paper.

Acknowledgements

National Research Foundation of Korea (NRF) (NRF-2020R1A2C2007077 and the Global Frontier Program CAMM-2019M3A6B3030638); KIST intramural grants (2N30520). The National Research Council of Science & Technology (NST) granted by the Ministry of Science, ICT & Future Planning (MSIP) (No. CRC-15-04-KIST);

Appendix A. Supplementary data

Supplementary data to this article can be found online at https://doi.org/10.1016/j.bios.2020.112663.

References

Agrawal, H.C., Davis, J.M., Himwich, W.A., 1968. Developmental changes in mouse brain: weight, water content and free amino acids. J. Neurochem. 15, 917–923. https://doi.org/10.1111/j.1471-4159.1968.tb11633.x.

Alfihed, S., Holzman, J.F., Foulds, I.G., 2020. Developments in the integration and application of terahertz spectroscopy with microfluidics. Biosens. Bioelectron. 165, 112393 https://doi.org/10.1016/j.bios.2020.112393.

Bowman, T., Bailey, K., El-shenawee, M., Bowman, T., Vohra, N., Bailey, K., El-shenawee, M., 2019. Terahertz tomographic imaging of freshly excised human breast tissues. J. Med. Imaging 6, 1. https://doi.org/10.1117/1.JMI.6.2.023501.

Darmo, J., Tamosiunas, V., Fasching, G., Kröll, J., Unterrainer, K., Beck, M., Giovannini, M., Faist, J., Kremser, C., Debbage, P., 2004. Imaging with a Terahertz quantum cascade laser. Optic Express 12, 1879. https://doi.org/10.1364/OPEX.12.001879.

Geng, Z., Zhang, X., Fan, Z., Lv, X., Chen, H., 2017. A route to terahertz metamaterial biosensor integrated with microfluidics for liver cancer biomarker testing in early stage. Sci. Rep. 7, 16378. https://doi.org/10.1038/s41598-017-16762-y.

Heo, C., Ha, T., You, C., Huynh, T., Lim, H., Kim, J., Kesama, M.R., Lee, J., Kim, T.-T., Lee, Y.H., 2020. Identifying fibrillization state of Aβ protein via near-field THz conductance measurement. ACS Nano. https://doi.org/10.1021/acsnano.9b08572.

Jeong, J., Kim, D., Seo, M., Kim, D.S., 2019. Strongly localized ohmic absorption of terahertz radiation in nanoslot antennas. Nano Lett. 19, 9062–9068. https://doi.org/10.1021/acs.nanolett.9b04117.

Ji, Y. Bin, Oh, S.J., Kang, S.-G., Heo, J., Kim, S.-H., Choi, Y., Song, S., Son, H.Y., Kim, S. H., Lee, J.H., Haam, S.J., Huh, Y.M., Chang, J.H., Joo, C., Suh, J.-S., 2016. Terahertz reflectometry imaging for low and high grade gliomas. Sci. Rep. 6, 36040. https://doi.org/10.1038/srep36040.

Kang, J.-H., Choe, J.-H., Kim, D.-S., Park, Q.-H., 2009. Substrate effect on aperture resonances in a thin metal film. Optic Express 17, 15652–15658. https://doi.org/10.1364/OE.17.015652.

Kang, J.-H., Kim, D.-S., Seo, M., 2018. Terahertz wave interaction with metallic nanostructures. Nanophotonics 7, 763–793. https://doi.org/10.1515/nanoph-2017-0093.

Kitahara, H., Yagi, T., Mano, K., Takeda, M.W., Kojima, S., Nishizawa, S., 2005. Dielectric characteristics of water solutions of ethanol in the terahertz region. J. Kor. Phys. Soc. 46, 82–85.

Lee, D.-K., Kang, J.-H., Kwon, J., Lee, J.-S., Lee, S., Woo, D.H., Kim, J.H., Song, C.-S., Park, Q.-H., Seo, M., 2017. Nano metamaterials for ultrasensitive Terahertz biosensing. Sci. Rep. 7, 8146. https://doi.org/10.1038/s41598-017-08508-7.

Lee, D.-K., Kang, J., Lee, J.-S., Kim, H.-S., Kim, C., Hun Kim, J., Lee, T., Son, J., Park, Q., Seo, M., 2015. Highly sensitive and selective sugar detection by terahertz nano-antennas. Sci. Rep. 5, 15459. https://doi.org/10.1038/srep15459.

Lee, D.-K., Yang, H., Song, H.S., Park, B., Hur, E.-M., Kim, J.H., Park, T.H., Seo, M., 2018a. Ultrasensitive terahertz molecule sensor for observation of photoinduced conformational change in rhodopsin-nanovesicles. Sensor. Actuator. B Chem. 273, 1371–1375. https://doi.org/10.1016/j.snb.2018.07.052.

Lee, J., Shmueli, K., Kang, B.T., Yao, B., Fukunaga, M., Van Gelderen, P., Palumbo, S., Bosetti, F., Silva, A.C., Duyn, J.H., 2012. The contribution of myelin to magnetic susceptibility-weighted contrasts in high-field MRI of the brain. Neuroimage 59, 3967–3975. https://doi.org/10.1016/j.neuroimage.2011.10.076.

Lee, J.W., Seo, M.A., Kang, D.H., Khim, K.S., Jeoung, S.C., Kim, D.S., 2007. Terahertz electromagnetic wave transmission through random arrays of single rectangular holes and slits in thin metallic sheets. Phys. Rev. Lett. 99, 137401 https://doi.org/10.1103/PhysRevLett.99.137401.

Lee, K., Jeoung, K., Kim, S.H., Ji, Y., Son, H., Choi, Y., Huh, Y.-M., Suh, J.-S., Oh, S.J., 2018b. Measuring water contents in animal organ tissues using terahertz spectroscopic imaging. Biomed. Optic Express 9, 1582. https://doi.org/10.1364/boe.9.001582.

Lee, S.-H., Choe, J.-H., Kim, C., Bae, S., Kim, J.-S., Park, Q.-H., Seo, M., 2020. Graphene assisted terahertz metamaterials for sensitive bio-sensing. Sensor. Actuator. B Chem. 310, 127841 https://doi.org/10.1016/j.snb.2020.127841.

Lee, S.-H., Lee, D., Choi, M.H., Son, J.-H., Seo, M., 2019. Highly sensitive and selective detection of steroid hormones using terahertz molecule-specific sensors. Anal. Chem. 91, 6844–6849. https://doi.org/10.1021/acs.analchem.9b01066.

Lim, C., Lee, S.-H., Jung, Y., Son, J.-H., Choe, J.-H., Kim, Y.J., Choi, J., Bae, S., Kim, J.H., Blick, R.H., Seo, M., Kim, C., 2018. Broadband characterization of charge carrier transfer of hybrid graphene-deoxyribonucleic acid junctions. Carbon N. Y. 130, 525–531. https://doi.org/10.1016/j.carbon.2018.01.049.

Meng, K., Chen, Tu-nan, Chen, Tao, Zhu, L., Liu, Q., Li, Zhao, Li, F., Zhong, S., Li, Ze-ren, Feng, H., Zhao, J., 2014. Terahertz pulsed spectroscopy of paraffin-embedded brain glioma. J. Biomed. Optic. 19, 077001 https://doi.org/10.1117/1.JBO.19.7.077001.

Neubrech, F., Huck, C., Weber, K., Pucci, A., Giessen, H., 2017. Surface-enhanced infrared spectroscopy using resonant nanoantennas. Chem. Rev. 117, 5110–5145. https://doi.org/10.1021/acs.chemrev.6b00743.

Oh, S.J., Kim, S.-H., Jeong, K., Park, Y., Huh, Y.-M., Son, J.-H., Suh, J.-S., 2013. Measurement depth enhancement in terahertz imaging of biological tissues. Optic Express 21, 21299–21305. https://doi.org/10.1364/OE.21.021299.

Park, H.-R., Ahn, K.J., Han, S., Bahk, Y.-M., Park, N., Kim, D.-S., 2013. Colossal absorption of molecules inside single terahertz nanoantennas. Nano Lett. 13, 1782–1786. https://doi.org/10.1021/nl400374z.

Qin, J., Xie, L., Ying, Y., 2016. A high-sensitivity terahertz spectroscopy technology for tetracycline hydrochloride detection using metamaterials. Food Chem. 211, 300–305. https://doi.org/10.1016/j.foodchem.2016.05.059.

Radde, R., Bolmont, T., Kaeser, S.A., Coomaraswamy, J., Lindau, D., Stoltze, L., Calhoun, M.E., Jäggi, F., Wolburg, H., Gengler, S., Haass, C., Ghetti, B., Czech, C., Hölscher, C., Mathews, P.M., Jucker, M., 2006. Aβ42-driven cerebral amyloidosis in transgenic mice reveals early and robust pathology. EMBO Rep. 7, 940–946. https://doi.org/10.1038/sj.embor.7400784.

Rahman, A., Rahman, A.K., Rao, B., 2016. Early detection of skin cancer via terahertz spectral profiling and 3D imaging. Biosens. Bioelectron. 82, 64–70. https://doi.org/10.1016/j.bios.2016.03.051.

Roh, Y., Lee, S.-H., Kang, B., Wu, J.W., Ju, B.-K., Seo, M., 2019. Terahertz optical characteristics of two types of metamaterials for molecule sensing. Optic Express 27, 19042. https://doi.org/10.1364/OE.27.019042.

Seo, M.A., Park, H.R., Koo, S.M., Park, D.J., Kang, J.H., Suwal, O.K., Choi, S.S., Planken, P.C.M., Park, G.S., Park, N.K., Park, Q.H., Kim, D.S., 2009. Terahertz field enhancement by a metallic nano slit operating beyond the skin-depth limit. Nat. Photon. 3, 152–156. https://doi.org/10.1038/nphoton.2009.22.

Serita, K., Matsuda, E., Okada, K., Murakami, H., Kawayama, I., Tonouchi, M., 2018. Terahertz microfluidic chips sensitivity-enhanced with a few arrays of meta-atoms. APL Photonics 3, 051603. https://doi.org/10.1063/1.5007681.

Shmueli, K., Dodd, S.J., Li, T.-Q., Duyn, J.H., 2011. The contribution of chemical exchange to MRI frequency shifts in brain tissue. Magn. Reson. Med. 65, 35–43. https://doi.org/10.1002/mrm.22604.

Wu, X., Quan, B., Pan, X., Xu, X., Lu, X., Gu, C., Wang, L., 2013. Alkanethiol-functionalized terahertz metamaterial as label-free, highly-sensitive and specific biosensor. Biosens. Bioelectron. 42, 626–631. https://doi.org/10.1016/j.bios.2012.10.095.

Xu, W., Xie, L., Zhu, J., Tang, L., Singh, R., Wang, C., Ma, Y., Chen, H.-T., Ying, Y., 2019. Terahertz biosensing with a graphene-metamaterial heterostructure platform. Carbon N. Y. 141, 247–252. https://doi.org/10.1016/j.carbon.2018.09.050.

Yamaguchi, S., Fukushi, Y., Kubota, O., Itsuji, T., Ouchi, T., Yamamoto, S., 2016. Brain tumor imaging of rat fresh tissue using terahertz spectroscopy. Sci. Rep. 6, 30124. https://doi.org/10.1038/srep30124.

Yan, X., Yang, M., Zhang, Z., Liang, L., Wei, D., Wang, M., Zhang, M., Wang, T., Liu, L., Xie, J., Yao, J., 2019. The terahertz electromagnetically induced transparency-like metamaterials for sensitive biosensors in the detection of cancer cells. Biosens. Bioelectron. 126, 485–492. https://doi.org/10.1016/j.bios.2018.11.014.

Yeo, W.G., Gurel, O., Srinivasan, N., King, P.D., Nahar, N.K., Park, S., Lehman, N.L., Sertel, K., 2017. Terahertz imaging and electromagnetic model of axon demyelination in Alzheimer's disease. IEEE Trans. Terahertz Sci. Technol. 7, 711–721. https://doi.org/10.1109/TTHZ.2017.2739481.

Yun, J., Oh, S.J., Song, K., Yoon, D., Son, H.Y., Choi, Y., Huh, Y.M., Rieh, J.S., 2017. Terahertz reflection-mode biological imaging based on InP HBT source and detector. IEEE Trans. Terahertz Sci. Technol. 7, 274–283. https://doi.org/10.1109/TTHZ.2017.2673549.

Zeng, S., Baillargeat, D., Ho, H.P., Yong, K.T., 2014. Nanomaterials enhanced surface plasmon resonance for biological and chemical sensing applications. Chem. Soc. Rev. 43, 3426–3452. https://doi.org/10.1039/c3cs60479a.